Mon. Not. R. Astron. Soc. **000**, 000–000 (0000) Printed 20 June 2014 (MN LATEX style file v2.2)

Formation of the First Low-Mass Stars from Cosmological Initial Conditions

Chalence Safranek-Shrader, Miloš Milosavljević, and Volker Bromm
Department of Astronomy, University of Texas at Austin, Austin, TX 78712, USA

arXiv:1401.0540v2 [astro-ph.GA] 11 Feb 2014

20 June 2014

ABSTRACT

We simulate the formation of a metal-poor ($10^{-2}\,Z_{\odot}$) stellar cluster in one of the first galaxies to form in the early Universe, specifically a high-redshift atomic cooling halo ($z \sim 14$). This is the first calculation that resolves the formation of individual metal-enriched stars in simulations starting from realistic cosmological initial conditions. We follow the evolution of a single dense clump among several in the parent halo. The clump forms a cluster of ~ 40 stars and sub-stellar objects within 7000 yrs and could continue forming stars ~ 5 times longer. Protostellar dust heating has a negligible effect on the star formation efficiency, at least during the early evolutionary stages, but it moderately suppresses gaseous fragmentation and brown dwarf formation. We observe fragmentation in thin gaseous filaments and sustained accretion in larger, rotating structures as well as ejections by binary interactions. The stellar initial mass function above $0.1\,M_{\odot}$, evaluated after $\sim 10^4\,\mathrm{yr}$ of fragmentation and accretion, seems in agreement with the recent measurement in ultra-faint dwarf spheroidal Galactic satellites of Geha et al. (2013).

Key words: galaxies: formation — galaxies: high-redshift — stars: formation

1 INTRODUCTION

Observations of low-metallicity stars in the stellar halo and satellites of the Milky Way have furnished an expanding window into how the Galaxy's primitive precursors formed and evolved in the ancient Universe. In a pursuit named "stellar archaeology," the chemical abundance patterns of metal-poor stars are used to expose the character of the supernovae that had enriched them and the physical state of their formation environment (e.g., Frebel et al. 2005; Karlsson et al. 2013). In particular, the metallicities and abundance patterns in the faintest and most metal-poor galaxies, the ultra-faint dwarf spheroidal satellites (UFDs), can potentially be used to probe the very first stellar generation forming from metal-free initial conditions and its immediate successors (Brown et al. 2012; Frebel & Bromm 2012; Vargas et al. 2013). Furthermore, there are hints that in the measured mass range, the stellar initial mass function (IMF) is shallower in UFDs than in more metal-rich and evolved galaxies (Geha et al. 2013), a potential challenge to star formation models and an important clue as to the origin of UFDs and of primitive, early stellar systems in general.

Capitalizing on the information provided by the fossils of the first galaxies requires a theoretical understanding of star formation under conditions distinct from those in the present Milky Way (e.g., Bromm 2013). Typical metallicities in UFDs are only $\sim 1\%$ of the solar value (e.g., Kirby et al. 2011). Current theory suggests that the first metal-enriched stellar generations formed in predominantly atomic gas clouds assembled by dark-matter-driven cosmic infall and thermal instability, and were subject to a temperature floor imposed by the cosmic microwave background (CMB) (e.g., Wise et al. 2012; Safranek-Shrader et al. 2014). In contrast, the bulk of present-day star formation, where recent numerical breakthroughs have focused (e.g., Bate 2012; Krumholz et al. 2012; Federrath & Klessen 2012), occurs in turbulent molecular clouds where the thermodynamics is dominated by dust and its coupling to the interstellar radiation field. Salient aspects of star formation in molecular clouds could apply to all systems with supersonic gas flow velocities, excluding star formation at extremely low or zero metallicities that operates in a distinct, Population III mode (e.g., Yoshida et al. 2006; Clark et al. 2011; Greif et al. 2011; Dopcke et al. 2013). These aspects include the formation of low-mass stars through turbulent gravitational fragmentation and of more massive stars through the coherent collapse of self-gravitating cores as well as (possibly "competitive") accretion stabilized by local protostellar radiative heating (Bate et al. 2003; Mac Low & Klessen 2004; McKee & Ostriker 2007; Zinnecker & Yorke 2007).

Our goal is to investigate the formation of the first generation of metal-enriched stars from cosmological initial conditions so that we can begin charting out the UFD formation history, relating it to concepts normally used to describe star formation under distinct, molecular-cloud-like conditions. We present highly zoomed adaptive-mesh-refinement (AMR) hydrodynamical simulations extending those in Safranek-Shrader et al. (2014) to much higher resolution, resolving the density and length scales where protostellar masses are imprinted. Namely, gaseous collapse in the presence of dust is now tracked to the densities $\sim 10^{13}\,\mathrm{cm}^{-3}$ where gas becomes optically thick to its cooling radiation and further fragmen-

© 0000 RAS

tation is strongly suppressed. We use Lagrangian sink particles to follow protostellar accretion after the initial collapse.

Importantly, the simulations here are derived from a section of a coarser simulation initialized from a realization of the ΛCDM cosmological model, instead of beginning from an artificially generated turbulent velocity field and spherically symmetric gas configuration. Therefore the gas flow morphology in the simulations here is a self-consistent outcome of turbulent virialization in a dark matter halo, thermal instability, and gravitational collapse.

2 METHODOLOGY

The simulations were performed with the AMR hydrodynamics code FLASH (Fryxell et al. 2000), version 4. The initial conditions were extracted from the highest metallicity cosmological simulation of Safranek-Shrader et al. (2014). The original cosmological simulation was performed in a 1 Mpc comoving box with standard ΛCDM metal-free initial conditions and an externally imposed H_2-dissociating UV background that prevented star formation in halos that have not reached the atomic cooling limit. Upon identifying an atomic cooling halo at $z = 13.8$, we endowed gas within its virial radius with a nonzero, uniform metallicity of $10^{-2}\,Z_\odot$, crudely mimicking enrichment by preceding Population III stars. The cooling by metallic fine structure lines induced localized gaseous collapse in the halo. Sink particles (hereafter "sinks") were allowed to form at densities $> 10^6\,\mathrm{cm}^{-3}$ and had accretion radii $\sim 10^4\,\mathrm{AU}$. Since fragmentation at still higher densities is expected on physical grounds, the sinks in Safranek-Shrader et al. (2014) did not represent individual stars, but pre-stellar clumps poised to form small stellar associations or clusters (Bergin & Tafalla 2007).

To study the formation and evolution of *individual* stars, much higher resolution is required to attain conditions at which the gas becomes optically thick to all forms of cooling radiation and further fragmentation is thermodynamically suppressed (unresolved fragmentation may still be possible in rotationally-supported protostellar disks). At the metallicity considered here and in the presence of dust, this occurs at a density $\sim 10^{12}\,\mathrm{cm}^{-3}$. Since achieving the requisite dynamical range in a full cosmological simulation is computationally prohibitive, we opted for the "cut-out" strategy, similar to Greif et al. (2011). When the maximum density in the $10^{-2}\,Z_\odot$ run of Safranek-Shrader et al. (2014) reached $10^7\,\mathrm{cm}^{-3}$, we extracted a cubical section of size $0.52\,\mathrm{pc}$ containing a total gas mass of $390\,M_\odot$ centered on the densest cell. The cut-out region contains a single, slightly ellipsoidal pre-stellar clump undergoing supersonic compression along one direction. The compression was produced by a collaboration of gravitational and pressure forces in the aftermath of thermal instability at densities $\sim 10^2 - 10^4\,\mathrm{cm}^{-3}$ in the parent simulation.

Since the gravitational potential was strongly gas-dominated we neglected the dark matter. We proceeded to integrate the cut-out simulation with a Jeans length resolution of at least 24 grid cells and subject to reflective hydrodynamical boundary that represented an approximately pressure-confined environment. However, we were careful to run the simulation only for a time much shorter than the sound crossing time from the box center to the boundary ($\approx 0.4\,\mathrm{Myr}$ at temperature $T = 50\,\mathrm{K}$), rendering the nature of the boundary condition immaterial. The gravitational potential of the gas was obtained with the multigrid solver with isolated gravitational boundary conditions. The simulations did not include magnetic fields, though we plan to explore their significance in future work.

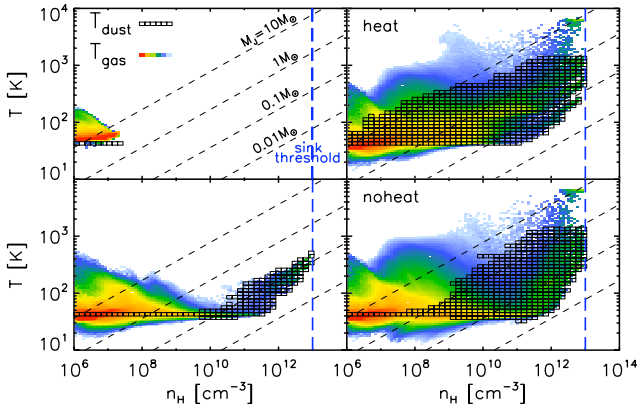

Figure 1. Density-temperature distribution of the gas (color from white to red scaling with gas mass) and dust (boxed points). Counterclockwise from top left, the panels show the beginning of the simulation, the onset of sink particle formation, and 7000 yr later in the simulations NOHEAT and HEAT. Dashed diagonals show lines of constant Jeans mass.

We inserted sinks when the density in a cell exceeded $n_{\rm sink} = 10^{13}\,\mathrm{cm}^{-3}$, the gas flow was converging $\nabla\cdot\mathbf{v} < 0$, the gravitational potential was a local minimum, and a small control volume around the cell was gravitationally bound. In practice, sink formation is preceded by Jeans instability in this highly compressed gas. Cells within the sink's accretion radius $r_{\rm acc} = 10\,\mathrm{AU} = 2.5\,\Delta x_{\rm min}$ with hydrogen densities $n_{\rm H} > n_{\rm sink}$ transferred a fraction $(n_{\rm H} - n_{\rm sink})/n_{\rm H}$ of their mass to the sink if the gas was gravitationally bound to the sink and had a radial velocity directed towards it. Here, $\Delta x_{\rm min}$ is the cell size at the highest level of grid refinement. We did not allow sinks to merge with each other. Sink particle motions were sub-cycled with a leapfrog scheme (for further details, see Federrath et al. 2010 and Safranek-Shrader et al. 2014).

We utilized the thermodynamical model and non-equilibrium chemical network described in Safranek-Shrader et al. (2010, 2012, 2014), now augmented with the dust processes in Omukai et al. (2005). The dust temperature, $T_{\rm d}$, was determined by grain thermal balance in the presence of thermal emission, heating by the CMB and protostellar radiation, and thermal coupling to the gas:

$$4\sigma_{\rm SB}(T_{\rm d}^4 - T_{\rm CMB}^4)\kappa_{\rm d}(T_{\rm d})\rho\beta_{\rm esc} = \frac{2k_{\rm B}(T_{\rm g} - T_{\rm d})n_{\rm d}}{t_{\rm coll}} + \sum_i \left(\frac{L_{{\rm acc},i}}{4\pi r_i^2}\right)\kappa_{\rm d}(T_{\rm d})\rho\beta_{\rm esc}, \quad (1)$$

where ρ is the gas density, $n_{\rm d}$ is the number density of dust grains, $T_{\rm g}$ and $T_{\rm CMB}$ are the gas and CMB temperatures, and $k_{\rm B}$ and $\sigma_{\rm SB}$ are the Boltzmann and Stefan-Boltzmann constants. The collision time between gas and dust particles is $t_{\rm coll}^{-1} = n_{\rm H}\sigma_{\rm d}\bar{v}_{\rm H} f$ where $\sigma_{\rm d}$ is the average dust grain cross-section, $\bar{v}_{\rm H}$ is the average speed of hydrogen nuclei, and $f \approx 0.4$ accounts for non-hydrogenic species (Schneider et al. 2006). The Planck mean opacity of dust grains, $\kappa_{\rm d}(T)$, was taken from Semenov et al. (2003) and we assumed linear scaling with metallicity. Thermal dust emission, which is a source of gas cooling through collisional coupling, was attenuated by a factor $\beta_{\rm esc} = \min(1, \tau_{\rm cont}^{-2})$, appropriate for optically-thick radiative diffusion (e.g., Masunaga et al. 1998). The continuum optical depth is given by $\tau_{\rm cont} = (\kappa_{\rm d} + \kappa_{\rm g})\rho L_{\rm J}$ where $L_{\rm J}$ is the Jeans Length, a local estimate for the physical extent of a gravitationally collapsing core, and $\kappa_{\rm g}$ is the metal-free gas Planck mean opacity (Mayer & Duschl 2005). To determine the metal fine-

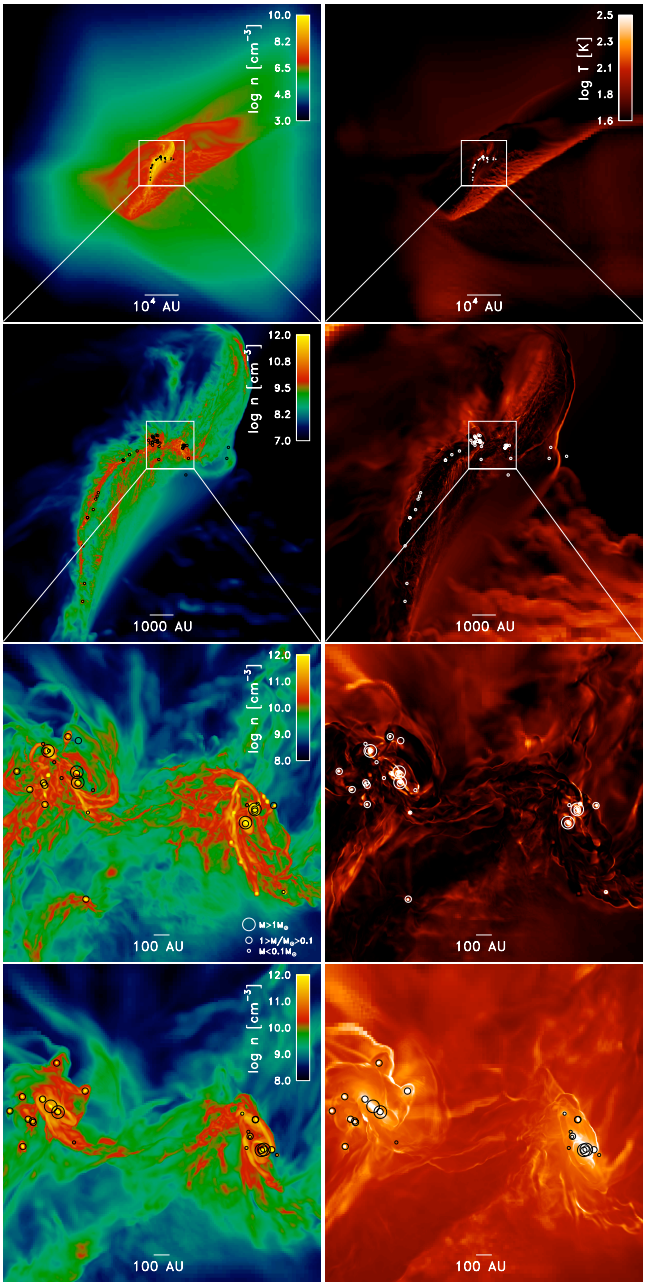

Figure 2. Mass-weighted line-of-sight projections of gas density (left column) and temperature (right column) at the end of NOHEAT (top three rows) and at the end of HEAT (bottom row). Circles denote sinks with the size increasing with sink mass. In the lower four panels, the smallest circles are sized with the sink accretion radius, $r_{\rm acc} = 10\,{\rm AU}$.

structure line cooling rates we iteratively calculated consistent line escape probabilities and level populations (e.g., Takahashi et al. 1983; Omukai 2000), using a local estimate of the Sobolev length, $L_{\rm sob} = c_{\rm s}/|\nabla \cdot \mathbf{v}|$, to approximate the size of the shielding region.

The summand in the last term of Equation 1 represents the heating by the radiation of the ith protostar located at distance r_i producing accretion luminosity $L_{{\rm acc},i} = GM_{*,i}\dot{M}_{*,i}/R_{*,i}$. By treating sinks as the sources of radiation, we took M_* to be the sink mass and $\dot{M}_*$ to be the sink accretion rate smoothed over a 10 yr ($\sim$ 30 hydrodynamical timesteps) period. This assumes that the luminosity is dominated by the accretion luminosity and that all

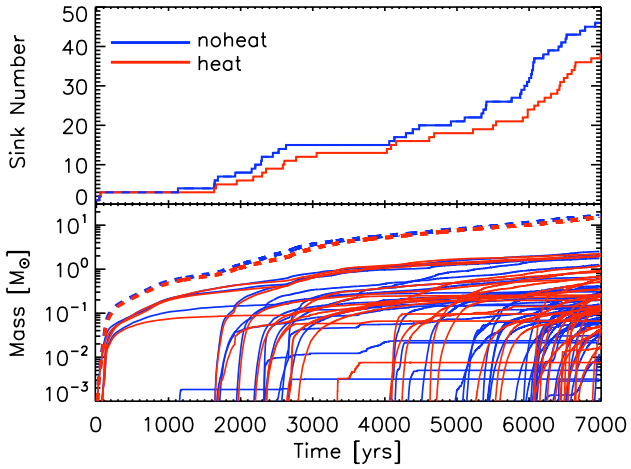

Figure 3. Number (upper panel) and masses (lower panel) of sink particles as a function of time since first sink formation in HEAT (red lines) and NOHEAT (blue lines). In the lower panel, solid and dashed lines show individual and total sink masses, respectively.

mass accreted by a sink is immediately and permanently incorporated into the protostar. We calculated the radius of the protostellar photosphere R_* with an analytic fit from Stahler et al. (1986), valid independent of metallicity for $M_* \lesssim 3\,M_\odot$ (e.g., Hosokawa & Omukai 2009).

3 RESULTS

We run a simulation HEAT that includes dust heating by protostellar radiation (via the last term in Eq. 1) and a reference simulation NOHEAT without heating. The thermodynamic evolution of gas and dust is shown in Figure 1. As the collapse proceeds, efficient fine-structure line cooling by [C II] and [O I] keeps the gas nearly isothermal at $T_{\rm CMB} \approx 40\,{\rm K}$ at densities $\lesssim 10^7\,{\rm cm}^{-3}$. Above this density, the lines become optically thick and the gas heats slightly, but cools back to $T_{\rm CMB}$ after reaching densities $\gtrsim 10^9\,{\rm cm}^{-3}$ where gas and dust collisionally couple. Isothermal collapse then continues until reaching densities $\sim 5 \times 10^{11}\,{\rm cm}^{-3}$. At these densities, marking the opacity limit for fragmentation, the continuum optical depth due to dust exceeds unity ($\beta_{\rm esc} \lesssim 1$, see Eq. 1), dust-cooling loses its efficacy, and the gas begins to evolve adiabatically. The effect of protostellar dust heating is minimal, mainly resulting in higher gas temperatures at densities $\gtrsim 10^8\,{\rm cm}^{-3}$ and a slight suppression of sink formation, consistent with the findings of Omukai et al. (2010).

When the gas reaches densities $\sim 10^{13}\,{\rm cm}^{-3}$ sink formation is possible based on the conditions described in Section 2. The first sink forms 4.3×10^4 yr after the beginning of the simulations and both are run for 7000 yr after this point. Figure 2 shows mass-weighted density and temperature projections at the end of both simulations. Sinks are forming over an extended $\sim 10^4$ AU-long filamentary structure, with thickness $\sim 1000\,{\rm AU}$ and density $\sim 10^8\,{\rm cm}^{-3}$. The structure is produced by a large-scale, supersonic colliding flow and is undergoing global gravitational collapse. We identify two sites of sink formation: in locally fragmenting filamentary structures, and in rotating, quasi-virialized disky flows produced by progressive global gravitational collapse of the filaments (as seen, respectively, in row 2 and rows 3 and 4 of Fig. 2).

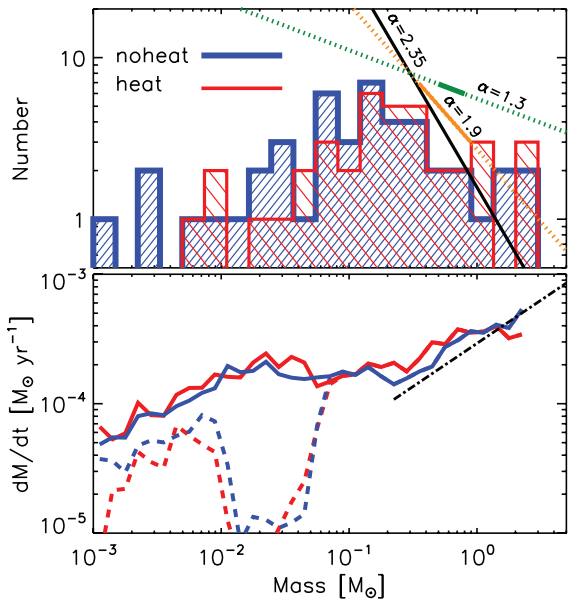

Figure 4. Upper panel: Sink particle mass function in HEAT (red line) and NOHEAT (blue line). Dashed lines show power-law IMF slopes $\alpha = 2.35$ (Salpeter), $\alpha = 1.9$ (in the Small Magellanic Cloud; Kalirai et al. 2013), and $\alpha = 1.3$ (the UFD Leo IV; Geha et al. 2013). The mass range over which the power-law slope was measured is indicated with a solid line. Lower panel: average sink accretion rate as a function of sink mass, including all sinks (dashed lines) and only accreting sinks (solid lines). The dot-dashed line shows the scaling $\dot{M}_\star \propto M_*^{2/3}$.

Figure 3 shows the total number of sinks and their individual masses. In NOHEAT, 46 sinks formed with a total mass of $16\,M_\odot$. In HEAT, 37 sinks formed with a total mass of $15\,M_\odot$. The average sink mass in both simulations is $M_{*,\rm tot}/N_{\rm tot} \approx 0.3-0.4\,M_\odot$ and median mass is $\approx 0.13\,M_\odot$. Sink binaries form in both simulations and we observe that binary interactions eject a number of low-mass sinks ($< 0.08\,M_\odot$) from the star forming region with velocities $3-7\,{\rm km\,s^{-1}}$. Figure 4 shows the average sink accretion rate as a function of mass. Sinks that are not ejected accrete at an average individual accretion rate of $2\times10^{-4}\,M_\odot\,{\rm yr^{-1}} \approx {\rm few}\times c_{\rm s}^3/G$ while their mass is in the range $0.01\,M_\odot < M_* < 0.3\,M_\odot$. At higher masses, the accretion rate increases approximately as $\dot{M}_* \propto M_*^{2/3}$ as sinks accrete from within the extended gaseous disks in which they are embedded. This trend continues up to the highest sink mass in NOHEAT, but in HEAT the increase of accretion rate with mass levels above $M_* \sim 0.7\,M_\odot$.

Figure 4 also shows the sink mass function at the end of both simulations. Because sinks do not instantaneously accrete their initial gravitationally unstable Jeans mass $\gtrsim 0.01\,M_\odot$, the simulations contain some sinks with very low masses that cannot be interpreted as fully fledged proto- or sub-stellar objects. The mass spectrum $dN/d\ln M_*$ in both simulations exhibits a broad peak at $M_* \sim (0.05-0.4)\,M_\odot$. The most massive sinks $M_* \approx 2.5\,M_\odot$ are located close to the centers of the densest disky structures (Fig. 2), already indicating hints of primordial segregation in the proto-stellar cluster.

4 DISCUSSION AND CONCLUSIONS

Studies that investigate the control of gravitational fragmentation in collapsing gas clouds using one-zone models, (e.g., Omukai et al. 2005, 2010; Schneider et al. 2006) assume that the fragmentation mass scale is set by the interplay of monolithic gravitational collapse and thermodynamics, neglecting large-scale, multi-dimensional gas motions. They predict that at the metallicity we consider, the characteristic fragmentation mass should be $\sim 0.5\,M_\odot$ as a result of gas-dust coupling at high densities $\gtrsim 10^8\,{\rm cm^{-3}}$. Since the Jeans mass $M_{\rm J} \propto \rho^{-1/2}$ and the compression at Mach number $\mathcal{M}$ results in a factor of $\mathcal{M}^2$ density enhancement, the characteristic mass should be revised downward by a factor $\sim 1/\mathcal{M}$. With the Mach number of the inflow into the fragmenting structure in the simulations being $\mathcal{M} \sim 3$, this revises the prediction of the one-zone models for the characteristic fragmentation mass to $\sim 0.1\,M_\odot$, consistent with the peak of our sink mass function. Models for gravitational fragmentation that do account for the underlying supersonically turbulent gas flow normally assume fully developed, statistically-homogeneous turbulence, as in molecular clouds, but potentially inapplicable in the present context, and idealized thermodynamic evolution (e.g., Padoan & Nordlund 2002).

A more definitive theoretical point of reference are simulations that resolve fragmentation into individual stars, albeit in a variety of contexts widely different from ours (e.g., Milky Way disk, metal-free or ultra-low-metallicity minihalos, etc.). Clark et al. (2008) and Dopcke et al. (2013) studied the onset of sink formation in clouds initialized with imposed turbulent velocity fluctuations at very low metallicities ($\leqslant 10^{-4}\,Z_\odot$), and followed the evolution of the cluster for only up to few hundred years. They identified gas-dust thermal coupling as the trigger of the conclusive fragmentation episode in this regime. Bate (2012) and Krumholz et al. (2012) carried out longer-duration integrations, also in clouds with imposed turbulent density fluctuations, designed to model the formation of small star clusters at $Z = Z_\odot$, both including protostellar radiative feedback. They found that the peak and shape of the resulting IMF are delicate functions of protostellar feedback and of how turbulence is introduced (Krumholz et al. 2012).

An isolated sink will accrete its initial Jeans mass, but a sink interacting with other matter (e.g., being subject to a tidal field, becoming a member of a binary system, or being ejected via a $\geqslant 3$ body interaction) may fail to attain the Jeans mass. The most massive sinks at the end of the simulations owe their status to sustained accretion, at a typical average rate of $\sim 4\times10^{-4}\,M_\odot\,{\rm yr^{-1}}$. The sites of this sustained accretion are the disky structures, mentioned in Section 3 and previously reported by Clark et al. (2008), in which shearing seems as important as turbulence. Various theoretical models for continued accretion after a core has accreted its initial Jeans mass typically predict a dependence of the mass accretion rate on the protostellar mass $\dot{M}_* \propto M_*^\xi$ (e.g., McKee & Tan 2003). Tentatively we find $\xi \approx 2/3$ at least in the range of stellar masses in which our two simulations agree. At higher masses $> 1\,M_\odot$ local protostellar heating in an increasingly crowded environment may be depressing Bondi-Hoyle accretion onto the most massive sinks. If the long-term accretion rate does remain at $\sim 2\times10^{-4}\,M_\odot\,{\rm yr^{-1}}$, the cluster will form a $\sim 20\,M_\odot$ star in $\sim 10^5\,{\rm yr}$ with the potential to produce an H II region that could truncate star formation.

The present simulation resolves small-scale fragmentation in only one of several (9 forming within $\sim 3\,{\rm Myr}$) pre-stellar clumps satisfying the conditions for gravitational collapse and star formation in the parent cosmological simulation. The other clumps would likely undergo a similar small scale evolution, implying that the total number of sinks, and thus stars, in a single episode of star formation could be an order of magnitude larger. More-

over, a single clump, like the one followed here for $7000\,\mathrm{yr}$ after initial sink formation, will continue infall on a dynamical time $\sim 3 \times 10^4\,\mathrm{yr}$, roughly five times longer than integrated here, producing $\sim 5 \times 40 = 200$ stars in one pre-stellar clump, or ~ 2000 stars in the whole halo. This value is interestingly consistent with the stellar masses of the faintest UFDs, Boötes II, Segue I & II, and Willman I. The surrounding halo at the time of star formation contains $\approx 2 \times 10^5\,M_\odot$ of dark matter within a reference radius of $30\,\mathrm{pc}$, furthermore consistent with the stellar-kinematics-inferred dynamical masses of these UFDs (McConnachie 2012).

The coarse-grained sinks representing pre-stellar clumps in Safranek-Shrader et al. (2014) and the fine-grained ones representing individual stars in the present work occupy a highly compact spatial region ($\sim 1\,\mathrm{pc}$) in which the gravitational potential is strongly baryon-dominated, whereas the stars in UFDs occupy much more extended, dark-matter-dominated regions. Long term evolution will inevitably convert the compact baryon-dominated star cluster into a more diffuse, highly dark-matter-dominated one. We already observe ejections of low-mass sinks by dynamical interactions, similar to Bate (2012). Given the low total number of stars in the cluster ejections will undoubtedly continue, extending to stellar mass objects, as long as the cluster remains baryon-dominated. If the ejected stars do not escape the host dark matter halo they will predominantly reside at large, dark-matter-dominated galactocentric radii. Stellar mass loss will further increase the mass-to-light ratio.

The stellar IMF in two UFDs measured in the mass range $0.5\,M_\odot < M_* < 0.8\,M_\odot$ is shallower, $dN/dM_* \propto M_*^{-\alpha}$ with $\alpha = 1.3 - 1.4$ (Geha et al. 2013), than the IMF of the Milky Way ($\alpha = 2.3$; Kroupa 2001) and the Small Magellanic Cloud ($\alpha = 1.9$; Kalirai et al. 2013) in a similar mass range. While we emphasize that the stellar IMF in our simulations is still evolving at the end of each simulation, we do find that for $M_* > 0.1\,M_\odot$, a truncated Pareto distribution maximum likelihood estimate (Aban et al. 2006) yields $\alpha = 1.26 \pm 0.05$ (HEAT) and $\alpha = 1.41 \pm 0.09$ (NOHEAT), consistent with the Geha et al. (2013) values.

It should be kept in mind that at present it is not clear whether UFDs started forming low-mass stars before reionization, where they were subject only to a non-ionizing H_2-dissociating UV background, or if their first low-mass stars formed only in a patch of the Universe reionized by more massive neighboring halos. In the latter case, we expect a similar outcome in a more massive host halo, though possibly modified due to higher inflow velocities and larger clump accretion rates. Furthermore, an object already forming stars at $z \approx 14$ could have ended up being incorporated into the central part of the Milky Way, rather than remaining an orbiting satellite. One central issue to be resolved is which process terminated star formation in UFDs: internal feedback from star formation, photoevaporation by reionization, or ram pressure stripping during infall into a more massive Milky Way progenitor halo.

We will report on a more comprehensive set of simulations and test cases, including a detailed analysis of the role of turbulence, in forthcoming publications. We are entering a period of rapid discovery, where ever more realistic simulations and comprehensive stellar archaeological surveys promise a deeper understanding of our ancient cosmic origins.

ACKNOWLEDGMENTS

The authors thank Christoph Federrath, Marla Geha, John Wise, Kazu Omukai, Raffaella Schneider, Anna Frebel, and many others for useful discussions. We also thank an anonymous referee for helpful comments. The FLASH code was in part developed by the DOE-supported Flash Center for Computational Science at the University of Chicago. The authors acknowledge the Texas Advanced Computing Center at The University of Texas at Austin for providing HPC resources under XSEDE allocation TG-AST120024. CSS is grateful for support provided by the NASA Earth and Space Science Fellowship (NESSF) program. This study was supported in part by NSF grant AST-1009928 and by the NASA grant NNX09AJ33G.

REFERENCES

Aban I. B., Meerschaert M. M., Panorska A. K., 2006, J. Am. Stat. Assoc., 101, 270
Bate M. R., 2012, MNRAS, 419, 3115
Bate M. R., Bonnell I. A., Bromm V., 2003, MNRAS, 339, 577
Bergin E. A., Tafalla M., 2007, ARA&A, 45, 339
Bromm V., 2013, Reports on Progress in Physics, 76, 112901
Brown T. M. et al., 2012, ApJ, 753, L21
Clark P. C., Glover S. C. O., Klessen R. S., 2008, ApJ, 672, 757
Clark P. C., Glover S. C. O., Klessen R. S., Bromm V., 2011, ApJ, 727, 110
Dopcke G., Glover S. C. O., Clark P. C., Klessen R. S., 2013, ApJ, 766, 103
Federrath C., Banerjee R., Clark P. C., Klessen R. S., 2010, ApJ, 713, 269
Federrath C., Klessen R. S., 2012, ApJ, 761, 156
Frebel A. et al., 2005, Nat, 434, 871
Frebel A., Bromm V., 2012, ApJ, 759, 115
Fryxell B. et al., 2000, ApJS, 131, 273
Geha M. et al., 2013, ApJ, 771, 29
Greif T. H., Springel V., White S. D. M., Glover S. C. O., Clark P. C., Smith R. J., Klessen R. S., Bromm V., 2011, ApJ, 737, 75
Hosokawa T., Omukai K., 2009, ApJ, 691, 823
Kalirai J. S. et al., 2013, ApJ, 763, 110
Karlsson T., Bromm V., Bland-Hawthorn J., 2013, Rev. Mod. Phys., 85, 809
Kirby E. N., Lanfranchi G. A., Simon J. D., Cohen J. G., Guhathakurta P., 2011, ApJ, 727, 78
Kroupa P., 2001, MNRAS, 322, 231
Krumholz M. R., Klein R. I., McKee C. F., 2012, ApJ, 754, 71
Mac Low M.-M., Klessen R. S., 2004, Rev. Mod. Phys., 76, 125
Masunaga H., Miyama S. M., Inutsuka S.-I., 1998, ApJ, 495, 346
Mayer M., Duschl W. J., 2005, MNRAS, 358, 614
McConnachie A. W., 2012, AJ, 144, 4
McKee C. F., Ostriker E. C., 2007, ARA&A, 45, 565
McKee C. F., Tan J. C., 2003, ApJ, 585, 850
Omukai K., 2000, ApJ, 534, 809
Omukai K., Hosokawa T., Yoshida N., 2010, ApJ, 722, 1793
Omukai K., Tsuribe T., Schneider R., Ferrara A., 2005, ApJ, 626, 627
Padoan P., Nordlund Å., 2002, ApJ, 576, 870
Safranek-Shrader C., Agarwal M., Federrath C., Dubey A., Milosavljević M., Bromm V., 2012, MNRAS, 426, 1159
Safranek-Shrader C., Bromm V., Milosavljević M., 2010, ApJ, 723, 1568
Safranek-Shrader C., Milosavljević M., Bromm V., 2014, MNRAS, 438, 1669
Schneider R., Omukai K., Inoue A. K., Ferrara A., 2006, MNRAS, 369, 1437
Semenov D., Henning T., Helling C., Ilgner M., Sedlmayr E., 2003, AAP, 410, 611
Stahler S. W., Palla F., Salpeter E. E., 1986, ApJ, 302, 590
Takahashi T., Silk J., Hollenbach D. J., 1983, ApJ, 275, 145
Vargas L. C., Geha M., Kirby E. N., Simon J. D., 2013, ApJ, 767, 134
Wise J. H., Turk M. J., Norman M. L., Abel T., 2012, ApJ, 745, 50
Yoshida N., Omukai K., Hernquist L., Abel T., 2006, ApJ, 652, 6
Zinnecker H., Yorke H. W., 2007, ARA&A, 45, 481